Dyes and Pigments 92 (2012) 1132–1137

Contents lists available at SciVerse ScienceDirect

Dyes and Pigments

journal homepage: www.elsevier.com/locate/dyepig

Novel di-anchoring dye for DSSC by bridging of two mono anchoring dye molecules: A conformational approach to reduce aggregation

Reenu Sirohi[a], Dong Hee Kim[b], Soo-Chang Yu[b], Sang Hee Lee[b,*]

[a] Department of Chemistry, Vivekananda Institute of Technology, Jaipur, Rajasthan, India
[b] Department of Chemistry, Kunsan National University, Kunsan 573-701, Republic of Korea

ARTICLE INFO

Article history:
Received 4 July 2011
Received in revised form
3 September 2011
Accepted 6 September 2011
Available online 17 September 2011

Keywords:
DSSC
Di-anchoring dye
Bridging
Suppression of aggregation

ABSTRACT

Two mono anchoring dye molecules were bridged together to give a new di-anchoring bis-merocyanine dye which possessed a non-planar conformation on a TiO_2 surface, a feature that impedes intermolecular aggregation of the dye in the adsorbed state. This dye also showed enhanced molar absorptivity and increased adsorption on TiO_2. A dye sensitized solar cell based on the bis-merocyanine dye yielded enhanced power conversion efficiency of 6.1%.

1. Introduction

DSSCs have emerged as a prospective alternative to conventional silicon-based photovoltaic devices due to their low cost and versatility [1,2]. The most important part of a DSSC is the photo sensitizer. Though Ru-based sensitizers have achieved power conversion efficiencies up to 11% under AM 1.5 irradiation [3], their high cost and toxicity diverted the attention of researchers towards metal free organic dyes which are inexpensive, easily synthesized, and environment friendly [4]. In recent years, a considerable improvement has been made in the performance of DSSCs based on organic dyes [5]. However, the low conversion efficiency and low stability [5a] are important issues still to be resolved.

One of the major factors which affects the conversion efficiency and stability of DSSC is the binding strength of dye on the TiO_2 surface. Strong binding of the dye on TiO_2 not only improves adsorption but also induces efficient charge injection [6]. One of the drawbacks of most of the organic dye molecules is the presence of only one anchoring group which can be a reason for inferior performance as compared to Ru(II) sensitizers, where 1–4 anchoring groups are present for an efficient electron transfer [7]. Recently, several researchers have developed double/multi electron acceptor type organic sensitizers to address the above mentioned problem [8–12]. However, consideration of conformation while designing a molecule of double electron acceptor type has received only scant attention [12]. Preferential conformation of the dye on the TiO_2 surface is important in terms of the improvement of charge injection and reduction of the effect of back electron transfer processes by maintaining the large physical separation between photo-oxidized donor and photo-injected electrons [12].

Formation of aggregates on the TiO_2 surface is another drawback of organic dyes in DSSC. A common structural strategy for suppression of dye aggregation is the introduction of bulky group [13]. Another unique approach is bridging of two chromophores into a spiro configuration similar to Ru-dyes [12].

Therefore, keeping in mind the requirement of strong binding ability and reduced tendency towards aggregation, we designed and synthesized a novel dye **KS-5** by bridging of two **L1** dye molecules (Fig. 1). A unique feature of **KS-5** is its near cross-shaped conformation in the adsorbed state which minimizes aggregation. The presence of two anchoring group is another advantageous feature of **KS-5** which increases the binding strength of dye on TiO_2. Photovoltaic properties of **KS-5** were compared with those of **L1** [14,15] to study the effect of bridging on the performance in a dye sensitized solar cell.

---

* Corresponding author. Tel.: +82 63 469 4578; fax: +82 63 469 4571.
E-mail address: leesh@kunsan.ac.kr (S.H. Lee).

0143-7208/$ – see front matter © 2011 Elsevier Ltd. All rights reserved.
doi:10.1016/j.dyepig.2011.09.003

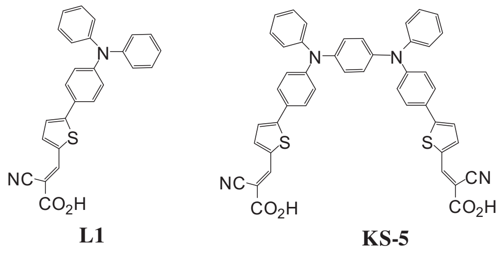

Fig. 1. Schematic structure of **L1** and **KS-5**.

2. Experimental section

2.1. Materials

The chemicals and solvents used in this work were obtained from commercial suppliers and were used without further purification unless otherwise noted. Parent dye, **L1** was synthesized according to procedure given in literature [14].

2.2. Synthesis

KS-5 was synthesized according to the synthetic route depicted in Scheme 1. It includes four general steps; amination of *p*-dibromobenzene with *N,N′*-diphenylphenylenediamine (**1P**) to give bisbromophenyl derivative **2P**, Suzuki coupling [14] of **2P** with 5-formyl-2-thiophene-boronic acid to afford the corresponding carbaldehyde **3P**, conversion of **3P** into its cyanoacrylate derivative **4P** by condensation with t-butyl cyanoacetate and subsequent hydrolysis of **4P** using trifluoroacetic acid afforded **KS-5**.

2.2.1. Synthesis of N^1,N^4-bis(4-bromophenyl)-N^1,N^4-diphenylbenzene-1,4-diamine (2P)

A mixture of *N,N′*-diphenyl-1,4-phenylenediamine (**1P**, commercially available) (500 mg, 1.92 mmol, 1 eq), 1,4 dibromobenzene (1.81 g, 7.68 mmol, 4 eq), sodium *tert*-butoxide (554 mg, 5.76 mmol, 3 eq), dppf (111 mg, 0.2 mmol, 1 eq) and Pd(OAc)$_2$ (18 mg, 0.0 8 mmol, 1 eq) in dry toluene (80 ml) was placed in a flask. Air was removed and it was heated under reflux under argon atmosphere for 8 h. After cooling to RT, the reaction was quenched by adding water, and then was extracted with ethyl acetate. The organic layer was dried over anhydrous MgSO$_4$ and evaporated under vacuum. The product was purified by silica gel column chromatography eluting first with hexane and then with hexane:toluene (7:1). White solid of **2P** was obtained (770 mg, 1.35 mmol, 70%). mp 228–229 °C. IR: 3082, 3056, 3033, 2922, 2351, 1596, 1582, 1505, 1484, 1308, 1270, 1069, 1004, 833, 815, 745, 693, 529, 520, 508. ^{1}H NMR (500 MHz, CDCl$_3$) δ7.32 (d, 4H, $J = 9$ Hz), 7.27 (dd, 4H, $J = 8$ Hz and 8 Hz), 7.08 (d, 4H, $J = 8$ Hz), 7.02 (t, 2H, $J = 8$ Hz), 6.96 (s, 4H), 6.95 (d, 4H, $J = 9$ Hz). ^{13}CNMR (125 MHz, CDCl$_3$) δ147.3, 146.9, 142.7, 132.1, 129.4, 125.5, 124.8, 124.1, 123.1, 114.6. HRMS (FAB) *m*/*z*: calcd. for $C_{30}H_{22}Br_2N_2$, 568.0149; found, 568.0143.

2.2.2. Synthesis of 5,5′-(4,4′-(1,4-phenylenebis(phenylazanediyl)) bis(4,1-phenylene)) dithiophene-2-carbaldehyde (3P)

To a solution of **2P** (500 mg, 0.876 mmol, 1 eq), PdCl$_2$(PPh$_2$)$_2$ (60 mg, 0.08 mmol, 0.1 eq) and dppf (48 mg, 0.08 mmol, 0.1 eq) in dry toluene (50 ml) was added a solution of 5-fomylthiophene-2-yl-2-boronic acid (274 mg, 1.75 mmol, 2 eq) and K$_2$CO$_3$ (725 mg, 5.25 mmol, 6 eq) in dry methanol (15 ml). The mixture was heated by microwave irradiation at 70 °C for 12 min. The reaction was quenched by the addition of water and extracted with ethyl acetate. The organic layer was dried over anhydrous MgSO$_4$ and filtered. Solvent removal by rotary evaporation followed by column chromatography on silica gel eluting first with toluene and then with hexane:ethyl acetate (4:1) gave **3P** as a yellow solid (310 mg, 0.49 mmol, 56%). mp 245–246 °C. IR: 3025, 2918, 2360, 2341, 1692, 1588, 1506, 1311, 1271. ^{1}H NMR (500 MHz, CDCl$_3$) δ9.84 (2H, s), 7.70 (d, 2H, $J = 4$ Hz), 7.53 (d, 4H, $J = 8.5$ Hz), 7.32 (dd, 4H, $J = 8$ Hz and 7.5 Hz), 7.30 (d, 2H, $J = 4$ Hz), 7.17 (d, 4H, $J = 8$ Hz), 7.09 (t, 2H, $J = 7.5$ Hz), 7.08 (d, 4H, $J = 8.5$ Hz), 7.05 (s, 4H). ^{13}CNMR (125 MHz, CDCl$_3$) δ182.6, 154.5, 148.9, 146.8, 142.7, 141.3, 137.8, 131.5, 129.5, 127.3, 126.1, 125.1, 123.9, 122.8, 122.1. HRMS (FAB) *m*/*z*: calcd. for $C_{40}H_{28}N_2O_2S_2$, 632.1592; found, 632.1586.

2.2.3. Synthesis of (2E,2′E)-tert-butyl 3,3′-(5,5′-(4,4′-(1,4-phenylenebis(phenylazanediyl))bis(4,1-phenylene))bis(thiophene-5,2-diyl))bis(2-cyanoacrylate) (4P)

A mixture of **3P** (200 mg, 0.316 mmol, 1 eq), *tert*-butyl cyanoacetate (180 mg, 1.26 mmol, 4 eq), ammonium acetate (96 mg, 1.26 mmol, 4 eq), and acetic acid (2 ml) in toluene was placed in a flask. Air was removed and the solution was heated under reflux under argon atmosphere for 45 min. After cooling, the reaction was

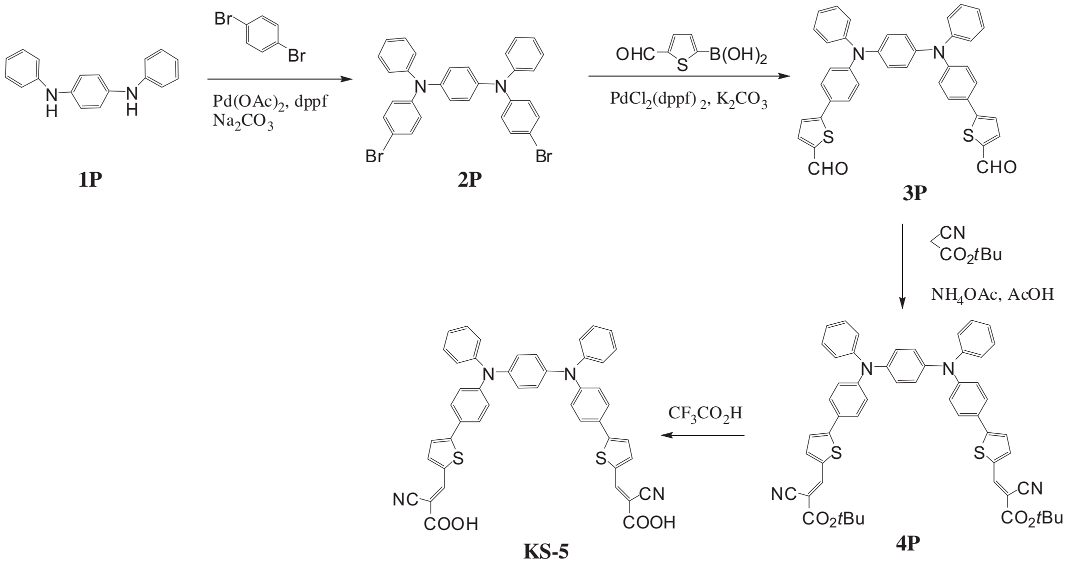

Scheme 1. Synthetic route for **KS-5**.

quenched by addition of water and extracted with ethyl acetate. The organic layer was dried over anhydrous $MgSO_4$ and evaporated under vacuum. The product was purified by silica gel column chromatography eluted with toluene. Orange solid of **4P** was obtained (248 mg, 0.284 mmol, 95%). mp 231–232 °C. IR: 3031, 2978, 2924, 2981, 2360, 2335, 2216, 1715, 1584, 1499, 1281, 1155. ^{1}H NMR (500 MHz, $CDCl_3$) δ8.18 (s, 2H), 7.69 (d, 2H, $J = 4$ Hz), 7.56 (d, 4H, $J = 9$ Hz), 7.32 (dd, 4H, $J = 8.5$ Hz and 7.5 Hz), 7.30 (d, 2H, $J = 4$ Hz), 7.17 (d, 4H, $J = 7.5$ Hz), 7.09 (t, 2H, $J = 8.5$ Hz), 7.08 (d, 4H, $J = 9$ Hz), 7.06 (s, 4H), 1.57 (s, 18H). ^{13}CNMR (125 MHz, $CDCl_3$) δ162.03, 154.3, 149.03, 149.01, 146.7, 145.7, 142.7, 138.9, 133.9, 129.5, 127.3, 126.1, 125.1, 123.9, 123.02, 122.09, 116.5, 98.7, 83.2, 28.02. HRMS (FAB) m/z: calcd. for $C_{54}H_{46}N_4O_4S_2$, 878.2960; found, 878.2966.

2.2.4. *Synthesis of (2E,2′E)-3,3′-(5,5′-(4,4′-(1,4-phenylenebis(phenylazanediyl))bis(4,1-phenylene))bis(thiophene-5,2-diyl))bis(2-cyanoacrylic acid) (**KS-5**)*

Compound **4P** (200 mg, 0.224 mmol) was stirred with trifluoroacetic acid (20 ml) for 15 min 200 ml of water was added and the resulting dark red solid **KS-5** (163 mg, 0.213 mmol, 95%) was collected by filtration. mp 288–289 °C. IR: 3443, 3032, 2923, 2958, 2963, 2345, 2215, 1685, 1571, 1492, 1436, 1412, 1316. ^{1}H NMR (500 MHz, DMSO-d_6), δ8.45 (s, 2H), 7.98 (d, 2H, $J = 4$ Hz), 7.68 (d, 4H, $J = 8.5$ Hz), 7.63 (d, 2H, $J = 4$ Hz), 7.38 (dd, 4H, $J = 8.5$ Hz and 7.5 Hz), 7.15 (m, 6H), 7.09 (s, 4H), 7.01 (d, 4H, $J = 8.5$ Hz). ^{13}CNMR (125 MHz, DMSO-d_6) δ164.2, 153.7, 149.08, 147.1, 146.6, 142.7, 142.3, 133.9, 130.3, 127.9, 126.8, 125.6, 125.4, 124.7, 124.3, 121.9, 117.08, 97.5. HRMS (FAB) m/z: calcd. for $C_{46}H_{30}N_4O_4S_2$, 766.17085; found, 766.1713.

2.3. *Instruments and characterizations*

^{1}H and ^{13}CNMR spectra were recorded on a Varian VNMRS 500 MHz NMR spectrometer. Mass spectra were obtained on a JMS-700, JEOL instrument operating in fast atom bombardment (FAB) mode. UV–Visible absorption spectra were measured on a Shimadzu UV-2401PC spectrophotometer. Fluorescence spectra were recorded on a SCINCO, FluoroMate FS-2 Fluorescence spectrophotometer. FTIR spectra were taken on a JASCO, 6300FV + IRT5000 spectrophotometer. Cyclic voltammogram was measured in DMSO:EtOH (1:1) solution containing 0.1 M TBA(PF6) with a scan rate of 50 mV s^{-1} using GCE (glassy carbon electrode) as working electrode, Pt wire as counter electrode and Ag/Ag^+ as reference electrode.

2.4. *Fabrication of DSSCs*

A paste consisting of 20 nm sized TiO_2 particles (CICC, PST-18NR) was applied with a scalpel on a fluorine-doped SnO_2 (FTO, Pilkington TEC-8 glass, 6–9 Ohms/sq with 2.3 mm thickness) conducting glass and then air-dried for 2 h. This TiO_2 film was gradually heated at 325 °C for 5 min, at 375 °C for 5 min, at 450 °C for 15 min, and at 500 °C for 15 min. Subsequently, a second scattering layer made up of a paste containing 400 nm anatase TiO_2 particles (CICC, PST-400C) was coated onto the first layer to form a light-scattering layer. The second layer was air-dried and then sintered in the same way as the first layer. The TiO_2 electrodes were immersed in 40 mM aqueous $TiCl_4$ solution at 70 °C for 30 min, washed with water and ethanol and heated at 500 °C for 30 min. After cooling to 80 °C, the TiO_2 electrodes were dipped into the dye solutions (0.4 mM for **L1** and 0.2 mM for **KS-5** in DMSO:ethanol (1:1) solvent) for 2 h. The dye-coated electrodes were rinsed quickly with ethanol. To prepare a Pt counter electrode, a small hole was drilled in a FTO glass and a drop of H_2PtCl_6 solution (2 mg Pt in 1 ml of ethanol) was placed on the FTO plate followed by sintering at 400 °C for 15 min. The dye-anchored TiO_2 electrodes and the Pt counter electrodes were assembled in to a sealed sandwich type cell using a thin Surlyn polymer transparent film (SX 1170-25, 25 μm) as a spacer between the electrodes. The sandwich cells were lightly compressed at 110 °C to seal the two electrodes. A thin layer of electrolyte was introduced into the inter electrode space from the counter electrode side through pre-drilled holes using vacuum backfilling method. Electrolyte contained 0.6 M 1-butyl-3-methylimidazolium iodide (BMII), 0.04 M I_2, 0.025 M LiI, 0.05 guanidinium thiocyanate (GUNCS), 0.25 M 4-*tert*-butylpyridine (TBP) in valeronitrile:acetonitrile (15:85). The holes were sealed with Surlyn and microscope cover slides to avoid leakage of the electrolyte solution.

2.5. *Photovoltaic characterization*

The current–voltage characteristics of the devices were carried out under simulated AM 1.5G irradiation using a xenon lamp-based solar simulator (Oriel 300 W solar simulator) attached to Kiethley 2400 source metre and calibrated with a crystalline silicon reference cell (VLSI standards, PVM-495-KG5). The solar cell efficiency (η) was obtained with the relation, $\eta = (J_{SC} \cdot V_{OC} \cdot FF)/P_{in}$, in which J_{SC} (mA cm^{-2}) is the current density measured at short circuit, V_{OC} (V) is the voltage measured at open circuit, FF is the fill factor and P_{in} is the input radiation power (for 1 sun illumination (AM 1.5G), $P_{in} = 100$ mW cm^{-2}). A black mask was applied to the area surrounding the TiO_2 with an illuminated active area of 0.159 cm^2 for all measurements.

3. Results and discussion

3.1. *Photophysical properties*

UV–Visible absorption spectrum of **KS-5** in DMSO:ethanol (1:1) solution (Fig. 2) exhibits a strong absorption band in the visible region. As expected, the absorption spectrum for **KS-5** is broader and red-shifted in comparison to that of **L1** due to the increased length of π-conjugation through phenylenediamine in **KS-5** (Fig. 2). The molar extinction coefficient ε of **KS-5** is more than twice as high as that of the parent dye **L1** (Table 1). The above observations indicate higher light absorption efficiency of **KS-5** as compared to parent dye **L1**.

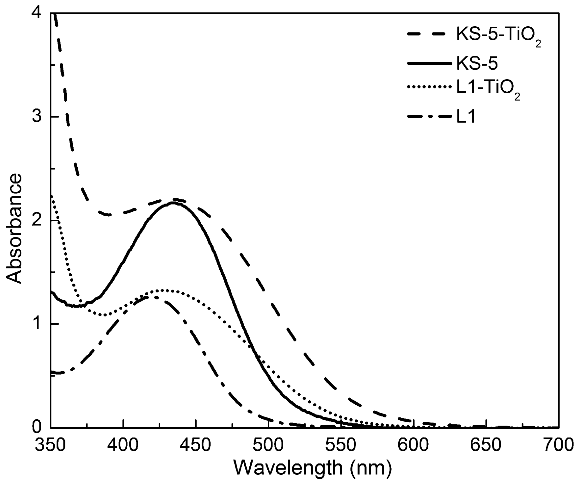

Fig. 2. Absorption spectra for **L1** and **KS-5** in DMSO:ethanol (1:1) solution and on TiO_2 film.

Table 1
Photophysical, electrochemical and photovoltaic performance data.

Dye	Absorption		Emission	Potentials and energy levels			Phtovoltaic performance data[d]			
	$\lambda_{abs}{}^{a}$/nm (ε/M^{-1} cm^{-1})	λ_{abs}/nm (on TiO$_2$)	$\lambda_{em}{}^{a}$ (nm)	E^{b}_{ox} (V)	E^{c}_{o-o} (V)	$E_{ox} - E_{o-o}$ (V)	J_{sc} (mA cm^{-2})	V_{OC} (mV)	*FF*	η (%)
L1	418 (23,760)	425	580	1.21	2.48	−1.27	9.3	616	0.73	4.2
KS-5	435 (50,483)	435	593	0.92	2.36	−1.46	13.4	646	0.70	6.1

Performances of DSSCs were measured with a 0.159 cm^2 working area.

[a] Absorption and emission spectra were measured in DMSO:ethanol (1:1) solution.

[b] The oxidation potentials were measured in DMSO:ethanol (1:1) solution containing 0.1 M tetrabutylammonium hexafluorophosphate (TBAPF$_6$) with a scan rate of 50 mV s^{-1} (vs NHE) using GCE (glassy carbon electrode) as working electrode, Pt wire as counter electrode and Ag/Ag$^+$ as reference electrode.

[c] E_{o-o} was determined from the intersection of absorption and emission spectra.

[d] The concentration was 0.4 mM for **L1** and 0.2 mM for **KS-5** in DMSO:ethanol (1:1) solution, with 0.6 M 1-butyl-3-methylimidazolium iodide (BMII), 0.04 M I$_2$, 0.025 M LiI, 0.05 GUNCS, 0.25 M 4-*tert*-butylpyridine (TBP) in valeronitrile:acetonitrile (15:85) as electrolyte and using 4.5 μm thick TiO$_2$ film.

3.2. Molecular conformation of **KS-5** on TiO$_2$ surface

As shown in Fig. 2, absorption spectra of dyes adsorbed on TiO$_2$ film are broadened which is a favourable spectral property for light harvesting of the solar spectrum. In addition to this, a slight red shift (418–425 nm) relative to that in solution, is observed for **L1** indicating partial *J*-type aggregation [16]. However, no such shift is observed for **KS-5** implying negligible *J*-type aggregation. This suppression of aggregation in **KS-5** may be ascribed to the non-planar geometry achieved by **KS-5** upon adsorption on TiO$_2$. In the free state, **KS-5** can have several conformations in equilibrium with each other. However, owing to its double anchoring mode, it possesses a non-planar conformation in the adsorbed state which reduces the possibility of intermolecular aggregation. Preferred conformation in double anchoring mode is presented in Fig. 3. As shown in Fig. 3b (side view), the orientation of the two D–π–A branches is not coplanar but twisted by an angle of 88.6°. Spatial separation (9.2 Å) between donor group and TiO$_2$ surface in **KS-5** is also sufficient to diminish the deleterious back electron transfer process.

In case of mono anchoring dye molecules, the preferential molecular orientation on the TiO$_2$ surface is perpendicular, however a fraction of the molecules may align horizontal next to the TiO$_2$ surface [17]. The possibility of this type of horizontal configuration in the adsorbed state is reduced in the case of **KS-5** due to the double anchoring behaviour, thereby slowing down the charge recombination process.

A clue for the double anchoring behaviour of **KS-5** was obtained by comparing the binding strength of **KS-5** on TiO$_2$ with that of **L1**. Desorption of **L1** from TiO$_2$ surface was achieved within 5 s by sonication in KOH methanol solution. However, complete removal of **KS-5** from TiO$_2$ surface required more than 5 min under identical conditions. The di-anchoring mode of **KS-5** was further confirmed by FTIR spectroscopy (Supplementary Material, Fig. S1). The C=O stretching band at 1685 assigned to the carboxylic acid groups of free **KS-5** was found to have disappeared in the IR spectrum of **KS-5** adsorbed on TiO$_2$ film, indicating the involvement of both carboxylic acid groups in adsorption on the TiO$_2$ surface; this result is similar to the observation made by Abbotto et al. [10] and Heredia et al. [12].

3.3. Amount of adsorption

The amount of the dyes adsorbed on TiO$_2$ film (4.5 μm) were then estimated by measuring the absorbance of desorbed dye solution. The concentration of **KS-5** (3.94×10^{-5} mmol/cm^2) was lower than that of **L1** (4.86×10^{-5} mmol/cm^2) but **KS-5** loaded a greater amount of D–π–A units ($2 \times 3.94 \times 10^{-5}$ mmol/cm^2) because one molecule of **KS-5** consists of two molecules of **L1** (Fig. 1). This result shows that strong binding of the dye can increase the adsorbed amount of dye on TiO$_2$ which in turn can increase the photocurrent. A common strategy to increase the amount of adsorption is the use of the thick TiO$_2$ films but it is well established that V_{oc} and fill factor decrease with increase in thickness of TiO$_2$ film [18]. Improved amount of adsorption for **KS-5** was due to strong binding and is therefore important in view of its application in solid state cells (SSDSSCs), where a thin film performs much better than a thicker film and optimum thickness lies in the range of 2–4 μm [19].

3.4. Molecular orbital calculations

Frontier molecular orbitals obtained by theoretical analysis (DFT, B3LYP/6-31G(d) level) (Fig. 4) showed that the HOMO of **KS-5** is located mostly on the *N,N′*-diphenylphenylenediamine and the LUMO is located on cyanoacrylic acid units, indicating an efficient photo induced electron transfer from dye to the TiO$_2$ electrode.

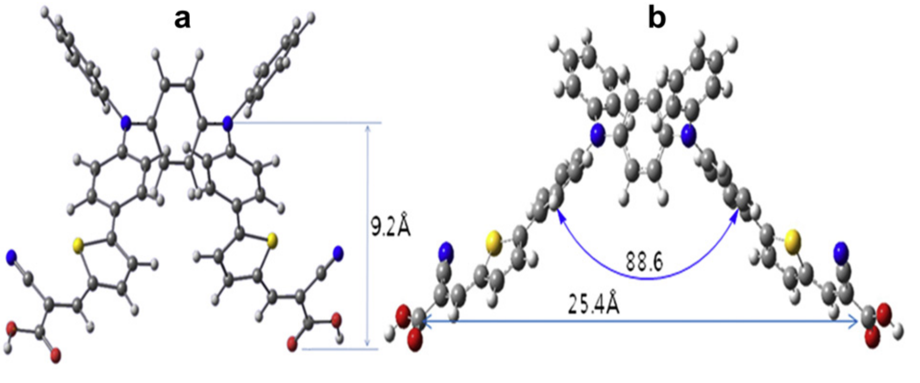

Fig. 3. Ground state geometry of **KS-5** calculated at B3LYP/6-31G(d): (a) front view; (b) side view.

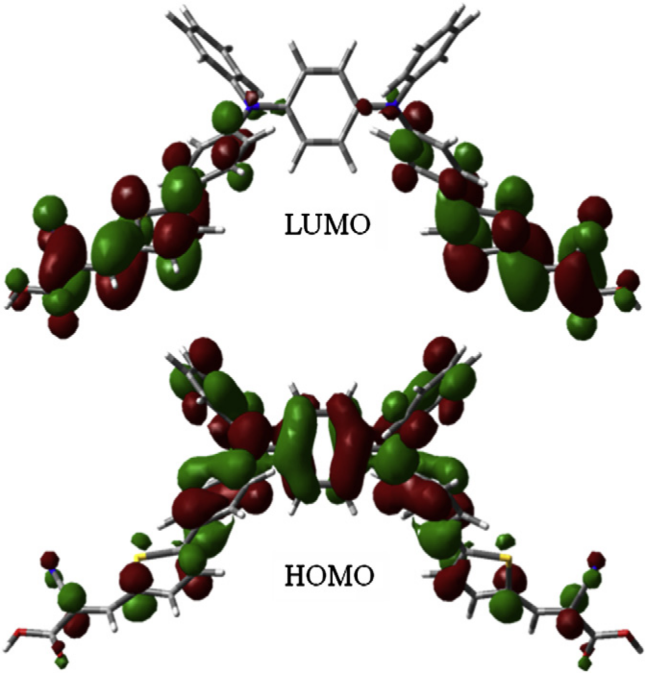

Fig. 4. HOMO–LUMO spatial orientation of **KS-5**.

3.5. Electrochemical properties

Redox potentials of dyes were measured by cyclic voltammetry (Supplementary Material, Figs. S2 and S3). The HOMO level of **KS-5** was found to be sufficiently lower than that of electrolyte pair I^-/I_3^- (0.4 V vs NHE) [20,21] and its LUMO level was sufficiently higher than conduction band edge of TiO_2 (−0.5 V vs NHE) [20,21], thereby indicating a favourable exothermic flow of charges throughout the photo-electronic conversion. A comparison of redox potentials of **KS-5** and **L1** revealed that E_{ox} and E_{o-o} of **KS-5** were lower than that of **L1** showing higher electron donating ability [21] of **KS-5** (Table 1).

3.6. Photovoltaic performance

The incident photon-to-current conversion efficiencies (IPCEs) of **L1** and **KS-5** are presented in Fig. 5. A solar cell based on **KS-5** showed the highest IPCE value, 87%, at 460 nm. It exhibited a broad IPCE spectrum with high IPCE values (>70%) from 400 to 540 nm. The IPCE spectrum of **L1** was however lower over the whole spectral region compared to **KS-5**, with maximum IPCE of 74% at 460 nm. Broad spectrum and higher IPCE values for **KS-5** reflect higher photocurrent and therefore better photovoltaic performance as compared to **L1**.

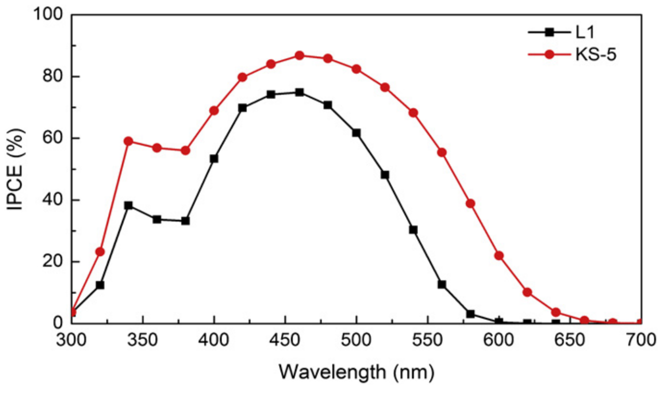

Fig. 5. The incident photon-to-current conversion efficiencies spectra for DSSCs based on **L1** and **KS-5**.

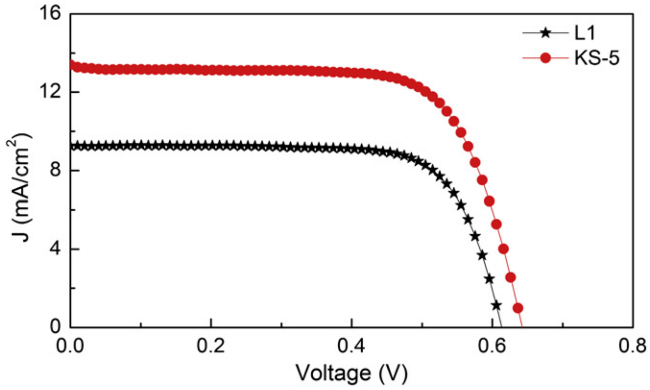

Fig. 6. Photocurrent–voltage curves for DSSCs based on **L1** and **KS-5**.

Fig. 6 shows the photocurrent–voltage (*J*–*V*) curves and photovoltaic performance data are listed in Table 1. Under standard global A.M. 1.5 solar condition, the **KS-5** sensitized solar cell with an active cell area of 0.159 cm^2 displayed a short circuit photocurrent density (J_{sc}) of 13.4 mA cm^{-2}, an open circuit voltage (V_{oc}) of 0.646 and a fill factor of 70.2 corresponding to an overall conversion efficiency (η) of 6.1%, while the DSSC based on parent dye **L1** showed lower J_{sc}, leading to a lower efficiency of 4.2%. Under different conditions (solvent and thickness of TiO_2 film) reported value of η for **L1** sensitized solar cell are 2.75% (3 μm) [14] and 5.2% (6 μm) [15].

4. Conclusions

We have synthesized and characterized a novel dye **KS-5** and demonstrated that appropriate bridging of two mono anchoring dye molecules can give several positive effects on photovoltaic performance. The di-anchoring moiety in **KS-5** caused strong binding to TiO_2 which not only increased the amount of adsorbed dye but also forced the dye molecule to assume a non-planar conformation, thereby minimizing aggregation. Furthermore, extended conjugated framework (through conjugate bridging) of **KS-5** gave a red-shifted and broadened spectrum as well as enhanced absorptivity as compared to parent dye **L1**. These factors led to about 1.5 times higher efficiency of **KS-5** (6.1%) compared to parent dye **L1** (4.2%).

Appendix. Supplementary material

Supplementary material associated with this article can be found, in the online version, at doi:10.1016/j.dyepig.2011.09.003.

References

[1] O'Regan B, Grätzel M. A low-cost, high-efficiency solar cell based on dye-sensitized colloidal TiO_2 films. Nature 1991;353:737–40.

[2] (a) Nazeeruddin Md K, Grätzel M. Dye-sensitized solar cells based on mesoscopic oxide semiconductor films. In: Ramamurthy V, Schanze K, editors. Molecular and supramolecular photochemistry, vol. 10. New York: Marcel-Dekker; 2002. p. 287–331;
(b) Asbury JB, Ellingson RJ, Gosh HN, Ferrere S, Notzig AJ, Lian T. Femtosecond IR study of excited-state relaxation and electron-injection dynamics of $Ru(dcbpy)_2(NCS)_2$ in solution and on nanocrystalline TiO_2 and Al_2O_3 thin films. Journal of Physical Chemistry B 1999;103(16):3110–9;
(c) Saito Y, Fukuri N, Senadeera R, Kitamura T, Wada Y, Yanagida S. Solid state dye sensitized solar cells using in situ polymerized PEDOTs as hole conductor.

Electrochemistry Communications 2004;6(1):71–4;
(d) Lee J-J, Coia GM, Lewis NS. Current density versus potential characteristics of dye-sensitized nanostructured semiconductor photoelectrodes. 1. Analytical expressions. Journal of Physical Chemistry B 2004;108(17):5269–81.

[3] (a) Nazeeruddin Md K, De Angelis F, Fantacci S, Selloni A, Viscardi G, Liska P, et al. Combined experimental and DFT-TDDFT computational study of photoelectrochemical cell ruthenium sensitizers. Journal of the American Chemical Society 2005;127(48):16835–47;
(b) Grätzel M. The advent of mesoscopic injection solar cells. Progress in Photovoltaics: Research and Applications 2006;14:429–42;
(c) Gao F, Wang Y, Zhang J, Shi D, Wang M, Baker RH, et al. A new heteroleptic ruthenium sensitizer enhances the absorptivity of mesoporous titania film for a high efficiency dye-sensitized solar cell. Chemical Communications 2008;23:2635–7.

[4] (a) Hara K, Wang Z-S, Sato T, Furube A, Katoh R, Sugihara H, et al. Oligothiophene-containing coumarin dyes for efficient dye-sensitized solar cells. Journal of Physical Chemistry B 2005;109(32):15476–82;
(b) Kim D, Lee JK, Kang SO, Ko J. Molecular engineering of organic dyes containing *N*-aryl carbazole moiety for solar cell. Tetrahedron 2007;63(9):1913–22;
(c) Chen Z, Li F, Huang C. Organic D-π-A dyes for dye-sensitized solar cell. Current Organic Chemistry 2007;11:1241–58.

[5] (a) Horiuchi T, Miura H, Uchida S. Highly-efficient metal-free organic dyes for dye-sensitized solar cells. Chemical Communications 2003;24:3036–7;
(b) Hagberg DP, Edvinsson T, Marinado T, Boschloo G, Hagfeldt A, Sun L. A novel organic chromophore for dye-sensitized nanostructured solar cells. Chemical Communications 2006;21:2245–7;
(c) Kuang D, Uchida S, Humphry-Baker R, Zakeeruddin S, Grätzel M. Organic dye-sensitized ionic liquid based solar cells: remarkable enhancement in performance through molecular design of indoline sensitizers. Angewandte Chemie, International Edition 2008;47(10):1923–7;
(d) Mishra A, Fischer MKR, Baurele P. Metal-free organic dyes for dye-sensitized solar cells: from structure: property relationships to design rules. Angewandte Chemie, International Edition 2009;48(14):2474–99.

[6] (a) Hagfeldt A, Grätzel M. Molecular photovoltaics. Accounts of Chemical Research 2000;33(5):269–77;
(b) Tian H, Yang X, Chen R, Zhang R, Hagfeldt A, Sun L. Effect of different dye baths and dye-structures on the performance of dye-sensitized solar cells based on triphenylamine dyes. Journal of Physical Chemistry C 2008;112(29):11023–33.

[7] De Angelis F, Fantacci S, Selloni A, Grätzel M, Nazeeruddin Md K. Influence of the sensitizer adsorption mode on the open-circuit potential of dye-sensitized solar cells. Nano Letters 2007;7(10):3189–95.

[8] Yang CH, Chen HL, Chuang YY, Wu CG, Chen CP, Liao SH, et al. Characteristics of triphenylamine-based dyes with multiple acceptors in application of dye-sensitized solar cells. Journal of Power Sources 2009;188(2):627–34.

[9] Park SS, Won YS, Choi YC, Kim JH. Molecular design of organic dyes with double electron acceptor for dye-sensitized solar cell. Energy and Fuels 2009;23(7):3732–6.

[10] Abbotto A, Manfredi N, Marinzi C, De Angelis F, Mosconi E, Yum J-H, et al. Di-branched di-anchoring organic dyes for dye-sensitized solar cells. Energy & Environmental Science 2009;2:1094–101.

[11] Mikroyannidis JA, Suresh P, Roy MS, Sharma GD. Triphenylamine- and benzothiadiazole-based dyes with multiple acceptors for application in dye-sensitized solar cells. Journal of Power Sources 2010;195(9):3002–10.

[12] Heredia D, Natera J, Gervaldo M, Otero L, Fungo F, Lin CY, et al. Spirobifluorene-bridged donor/acceptor dye for organic dye-sensitized solar cells. Organic Letters 2010;12(1):12–5.

[13] (a) Ning Zj, Zhang Q, Wu W, Pei H, Liu B, Tian H. Starburst triarylamine based dyes for efficient dye-sensitized solar cells. Journal of Organic Chemistry 2008;73(10):3791–7;
(b) Cho N, Choi H, Kim D, Song K, Kang MS, Kang SO, et al. Novel organic sensitizers containing a bulky spirobifluorene unit for solar cell. Tetrahedron 2009;65(31):6236–43.

[14] Hagberg DP, Edvinsson T, Marinado T, Boschloo G, Hagfeldt A, Sun L. Tuning the HOMO and LUMO energy levels of organic chromophores for dye sensitized solar cells. Journal of Organic Chemistry 2007;72(25):9550–6.

[15] Liu W-H, Wu I-Che, Lai C-H, Lai C-H, Chou Pi-Tai, Li Yi-T, et al. Simple organic molecules bearing a 3,4-ethylenedioxythiophene linker for efficient dye-sensitized solar cells. Chemical Communications 2008;41:5152–4.

[16] (a) Tsao M-H, Wu Tzi-Yi, Wang H-P, Sun I-W, Su S-Gang, Lin Y-Chung, et al. An efficient metal-free sensitizer for dye-sensitized solar cells. Materials Letters 2011;65(3):583–6;
(b) Liang M, Xu W, Cai F, Chen P, Peng B, Chen J, et al. New triphenylamine-based organic dyes for efficient dye-sensitized solar cells. Journal of Physical Chemistry C 2007;111(11):4465–72.

[17] Hahlin M, Johansson EMJ, Plogmaker S, Odelius M, Hagberg DP, Sun L, et al. Electronic and molecular structures of organic dye/TiO_2 interfaces for solar cell applications: a core level photoelectron spectroscopy study. Physical Chemistry Chemical Physics 2010;12:1507–17.

[18] (a) Kang MG, Ryu KS, Chang SH, Park NG, Hong JS, Kim K-J. Dependence of TiO_2 film thickness on photocurrent-voltage characteristics of dye-sensitized solar cells. Bulletin of the Korean Chemical Society 2004;25:742–4;
(b) Mathew A, Rao GM, Munichandraiah N. Effect of TiO_2 electrode thickness on photovoltaic properties of dye sensitized solar cell based on randomly oriented Titania nanotubes. Materials Chemistry and Physics 2011;127(1–2):95–101.

[19] (a) Fujishima A, Zhang X-T. Solid-state dye-sensitized solar cells. In: Soga T, editor. Nanostructured materials for solar energy conversion. Oxford, UK: Elsevier; 2006. p. 255–76;
(b) Araujo GL, Marti A. Absolute limiting efficiencies for photovoltaic energy conversion. Solar Energy Materials and Solar Cells 1994;33(2):213–40.

[20] Klein C, Nazeeruddin Md K, Censo DD, Liska P, Grätzel M. Amphiphilic ruthenium sensitizers and their applications in dye-sensitized solar cells. Inorganic Chemistry 2004;43(14):4216–26.

[21] Chang YJ, Chow TJ. Triaryl linked donor acceptor dyads for high-performance dye-sensitized solar cells. Tetrahedron 2009;65(46):9626–32.